Theoretical treatment of the interaction between two-level atoms and periodic waveguides

Xiaorun Zang, Philippe Lalanne

HAL Id: hal-01381376
https://hal-iogs.archives-ouvertes.fr/hal-01381376

Submitted on 14 Oct 2016

Optics Letters

Theoretical treatment of the interaction between two-level atoms and periodic waveguides

Xiaorun Zang and Philippe Lalanne*

Laboratoire Photonique Numérique et Nanosciences, Institut d'Optique d'Aquitaine, Université Bordeaux, CNRS, 33405 Talence, France
*Corresponding author: philippe.lalanne@institutoptique.fr

Light transport in periodic waveguides coupled to two-level atoms is investigated theoretically. By using optical Bloch equations and a photonic modal formalism, we derive a convenient semi-analytical expression for calculating the scattering matrix of single atoms trapped in periodic waveguides. The expression that holds for both photonic and plasmonic waveguides represents a basic building block toward the study of collective effects arising from photon-mediated multi-atom interactions in periodic waveguides. © 2015 Optical Society of America

Nanophotonic structures are routinely used to enhance light-matter interactions by modifying the density of virtual photon states. New hybrid quantum systems, combining cold atoms and nanostructured devices, have recently emerged. The combination of excellent quantum-coherent properties with a very flexible platform for implementing strong interactions at sub-wavelength scales is expected to go beyond classical settings of all-solid-state QED with quantum dots [1]. Examples include ultra-thin unclad optical fibers [2–4], photonic-crystal cavities [5], and more recently photonic periodic waveguides, for which the strong field enhancement at the band edge bears a high potential for atom-photon interaction [6,7].

Collective effects mediated by guided light in hybrid waveguides arise from multiple scattering between distant atoms through guided photons. Potentially any geometry can be analyzed provided that one knows propagating operators between atom pairs, scattering operators of individual atoms, and termination operators that describes how light is scattered at the waveguide facets. Indeed, modal formalisms that describe all the operators in the natural electromagnetic eigenstates (Bloch modes) of the waveguide are ideally suited to analyze collective phenomena in macroscopic-hybrid waveguides that represent a real challenge for numerical methods that rely on a full discretization of Maxwell's differential equations. Bloch-mode formalisms for propagation and termination operators have already been successfully developed in the context of light localization in photonic-crystal waveguides [8–10]. Here

we expand this work, present a theoretical derivation of the scattering matrix of one atom [11], and propose semi-analytical expressions that can be easily calculated. The derivation accurately considers the phase of transmitted and reflected photons, the saturation of the atom for multiphoton incident states, and radiation due to imperfect atom-waveguide couplings.

We maintain the theoretical discussion at a general level, potentially with waveguides composed of lossy and dispersive materials. The sole assumption is that the waveguide is made of reciprocal material. The scattering-matrix derivation can be performed with a semi-classical formalism, but we rely here on a fully quantum treatment including a quantization of the atom and photon field. The approach is based on a combination of electromagnetic Bloch-mode-expansion techniques [12] with the optical Bloch equations for the atom density-matrix operator [13]. The former provides an accurate electromagnetic description of the system, including the local electric field and local density of electromagnetic states, and the latter allows us to describe the population evolution of the quantum system, assumed to be a two-level system. Both formalisms are already documented in the literature, and we do not present them again hereafter. Rather, we focus on how they are coupled to obtain the scattering matrix expression. The derivation is inspired from earlier theoretical works on the coupling of quantum emitters with *translation-invariant* dielectric [11,14,15] or metallic [16,17] waveguides, and coupled-resonator guides [18,19].

Let us assume that the atom is not in motion and can be considered as a two-level system with ground and excited states ($|g\rangle$, $|e\rangle$) separated by frequency ω_A, and that it is initially in the ground state. The atom is driven at frequency ω_L by a coherent laser field $\mathbf{E}_{inc} = \alpha \tilde{\mathbf{E}}^{(1)}(\mathbf{r}, \omega_L)$, with $\tilde{\mathbf{E}}^{(1)}$ the normalized fundamental forward-propagating Bloch mode of the waveguide ($|\alpha|^2$ represents the power flow of the driving field); see Fig. 1.

The interaction between the photons and the atom is described by a classical Hamiltonian:

$$\hat{H} = \int d^3\mathbf{r} \int_0^\infty \hat{\mathbf{f}}^+(\mathbf{r}, \omega)\hat{\mathbf{f}}(\mathbf{r}, \omega)\hbar\omega d\omega$$
$$+ \frac{1}{2}\hbar\omega_A \hat{\sigma}_z - [\mu \cdot \hat{\mathbf{E}}^-(\mathbf{r}_A)\hat{\sigma} + \hat{\sigma}^+ \hat{\mathbf{E}}^+(\mathbf{r}_A) \cdot \mu]. \quad \textbf{(1)}$$

The first term describes the electromagnetic field and the media, with $\hat{\mathbf{f}}(\mathbf{r}, \omega)$ and $\hat{\mathbf{f}}^+(\mathbf{r}, \omega)$ the bosonic vector field operators for the elementary excitations of the system; the second term
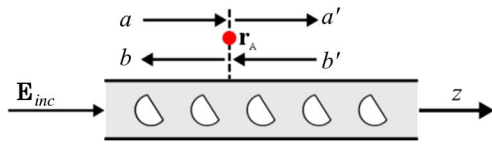
Fig. 1. Schematic of the hybrid system. An atom at $\mathbf{r}_A$ trapped near a periodic waveguide (made from reciprocal materials) and initially in its ground state. It is driven by a guided multiphoton coherent state $\mathbf{E}_{\text{inc}}$ propagating forward at frequency ω_L. The scattering matrix for one atom [Eq. (6)] relates the scattered amplitudes, a' and b, of the Bloch mode to the incident ones, a and b'.

accounts for the energy of the atom, with $\hat{\sigma}_z = |e\rangle\langle e| - |g\rangle\langle g|$ being the population difference operator; the third term accounts for the interaction between the atom and the total electric field, $\boldsymbol{\mu}$ being the transition electric dipole moment and $\hat{\sigma}$ the coherence operator. The electric field operator $\hat{\mathbf{E}}^+(\mathbf{r}_A)$ at the position $\mathbf{r}_A$ of the atom consists of three contributions: the vacuum field operator, the quantized emission field of the atom, whose main ingredients are driven by the imaginary part of the classical Green tensor of the periodic waveguide and the bosonic vector field operators, and the externally driving field. By assuming that the driving field is not just a single photon, but a coherent state at frequency ω_L that can be treated as a classical complex field, the nonlinear response of the atom can be formally mapped to an external Rabi frequency into the optical Bloch equations; see details in [20] and in the method section in [16]. Under the rotating wave approximation, the dynamics of the expectation values is given by optical Bloch equations, and the expectation value of the total (coherent) field operator at the laser frequency can be casted into two terms [13]:

$$\langle \mathbf{E}(\mathbf{r}) \rangle = \mathbf{E}_{\text{inc}}(\mathbf{r}) + \langle \mathbf{E}_{\text{at}}(\mathbf{r}) \rangle, \qquad (2)$$

where $\langle \mathbf{E}_{\text{at}}(\mathbf{r}) \rangle$ is the expectation value of the field radiated by the atom. This general result that is valid for weak atom-field coupling regimes is not restricted to our specific waveguide geometry [13]. If one further neglects the frequency shift (the Lamb shift in a vacuum electromagnetic environment) due to the self-action of the induced dipole and decoherence effects, the Rabi frequency depends only on the driving laser field at the atom position, and the expectation value for the induced dipole moment reads as

$$\langle \mathbf{d} \rangle = \frac{-2|\boldsymbol{\mu}|^2}{\hbar} \mathbf{E}_{\text{inc}}(\mathbf{r}_A, \omega_L) \frac{(2\delta - j\gamma)}{4\delta^2 + 2|\Omega|^2 + \gamma^2}, \qquad (3)$$

where $\delta = \omega_L - \omega_A$ is the detuning between the laser and atom frequencies, $\gamma = 2\omega_L^2 |\boldsymbol{\mu}|^2/(\varepsilon_0\hbar)\mathbf{u}^t \cdot \text{Im}(\mathbf{G}(\mathbf{r}_A, \mathbf{r}_A, \omega_L)) \cdot \mathbf{u}$ denotes the modified spontaneous decay rate of the excited state [13], ε_0 the vacuum permittivity, and $\Omega = (2\boldsymbol{\mu}/\hbar)\mathbf{u} \cdot \mathbf{E}_{\text{inc}}$ is the complex external Rabi frequency. In the previous expressions, $\mathbf{u}$ denotes the polarization unit vector $\mathbf{E}_{\text{inc}} = E_{\text{inc}}\mathbf{u}$ of the photon at the atom position, and $\mathbf{G}(\mathbf{r}, \mathbf{r}', \omega_L)$ is the Green tensor in the presence of the waveguide, corresponding to the electric field response at $\mathbf{r}$ to a point dipole current source at $\mathbf{r}'$.

To solve for Eqs. (2) and (3), we expand the field radiated by the atom in the complete set of optical Bloch modes, including a discrete set of truly guided modes and a continuum of

radiation modes. The expectation value of the total field operator is written as

$$z > z_A, \quad \langle \mathbf{E}(\mathbf{r}) \rangle = \sum_{p=1,N} \alpha t_p \tilde{\mathbf{E}}^{(p)}(\mathbf{r}) + \text{continuum}, \qquad (4a)$$

$$z < z_A, \quad \langle \mathbf{E}(\mathbf{r}) \rangle = \alpha \tilde{\mathbf{E}}^{(1)}(\mathbf{r}) + \sum_{p=1,N} \alpha r_p \tilde{\mathbf{E}}^{(-p)}(\mathbf{r}) + \text{continuum},$$

$$\qquad (4b)$$

where z_A is the z-coordinate of the atom, r_p and t_p are the reflection and transmission amplitude coefficients, and p and N denote the label and the number of truly guided modes, respectively. To calculate the amplitude coefficients, one relies on a biorthogonal form that handles the orthogonality between bound and continuum states. The form can be mathematically derived from Maxwell's equations with Lorentz reciprocity theorem, with some theoretical difficulties for the continuum states that are well documented in textbooks on waveguides [21]. It was generalized to periodic waveguides in [12], and by introducing complex spatial coordinate transforms that map the open problem with the associated continuum of radiation states to a closed problem with a countable number of discrete states, called quasi-normal Bloch modes (QNBMs), the theoretical difficulties are removed in the numerical implementation. Thus the formalism accurately accounts for coupling to radiations modes.

We conveniently normalize the QNBMs such that $\int [\tilde{\mathbf{E}}^{(-p)}(\mathbf{r}) \times \tilde{\mathbf{H}}^{(p)}(\mathbf{r}) - \tilde{\mathbf{E}}^{(p)}(\mathbf{r}) \times \tilde{\mathbf{H}}^{(-p)}(\mathbf{r})] \cdot d\mathbf{S} = 4P$, where the integral is performed over any cross-section plane of the waveguide and $P = 1$. For truly guided Bloch modes operating below the cladding light line and for nonabsorbent materials, $\tilde{\mathbf{E}}^{(-p)} = -(\tilde{\mathbf{E}}^{(p)})^*$ and $\tilde{\mathbf{H}}^{(-p)} = (\tilde{\mathbf{H}}^{(p)})^*$, such that guided Bloch-modes have unit power flow. With this normalization, the scattering coefficients are obtained by considering that the atoms act as electric-dipole sources whose radiation emission feeds the waveguide QNBMs, and we have $\alpha t_p = (j\omega_L/4P)\langle \mathbf{d} \rangle \cdot \tilde{\mathbf{E}}^{(-p)}(\mathbf{r}_A) + \delta(p)$, with $\delta(p) = 1$ if $p = 1$ and 0 otherwise and $\alpha r_p = (j\omega_L/4P)\langle \mathbf{d} \rangle \cdot \tilde{\mathbf{E}}^{(p)}(\mathbf{r}_A)$ [12]. Using $\langle \mathbf{d} \rangle$ from Eq. (3), we obtain

$$t_p = \sigma_0 \frac{-j\varepsilon_0 c}{4P} \frac{\gamma_0(2\delta_L - j\gamma)}{4\delta_L^2 + 2|\Omega|^2 + \gamma^2} \tilde{\mathbf{E}}^{(1)}(\mathbf{r}_A) \cdot \tilde{\mathbf{E}}^{(-p)}(\mathbf{r}_A) + \delta(p),$$

$$\qquad (5a)$$

$$r_p = \sigma_0 \frac{-j\varepsilon_0 c}{4P} \frac{\gamma_0(2\delta_L - j\gamma)}{4\delta_L^2 + 2|\Omega|^2 + \gamma^2} \tilde{\mathbf{E}}^{(1)}(\mathbf{r}_A) \cdot \tilde{\mathbf{E}}^{(p)}(\mathbf{r}_A), \qquad (5b)$$

where $\sigma_0 = 6\pi c^2/\omega_A^2$ denotes the extinction cross-section on resonance of an isolated two-level system, and $\gamma_0 = \omega_A^3 |\boldsymbol{\mu}|^2/(3\pi\varepsilon_0\hbar c^3)$ is the natural decay rate of the atom in a vacuum (c is the light speed). Equations (5a) and (5b), which constitute the main result of the present work, are general expressions that are valid for any photonic or plasmonic waveguides. They can be extended to incorporate dephasing and nonradiative decays [13].

For atoms with prescribed quantization axes (or oriented molecules), the induced dipole is not parallel to the incident electric field. This important case can be treated as well by replacing $|\boldsymbol{\mu}|^2\mathbf{E}_{\text{inc}}$ by $(\boldsymbol{\mu} \cdot \mathbf{E}_{\text{inc}})\boldsymbol{\mu}$ in Eq. (3) with slightly modified expressions for γ and Ω, $\gamma = 2\omega_L^2/(\varepsilon_0\hbar)\boldsymbol{\mu}^{*t} \cdot$

$\text{Im}(\mathbf{G}(\mathbf{r}_A, \mathbf{r}_A, \omega_L)) \cdot \boldsymbol{\mu}$ and $\Omega = (2/\hbar)\boldsymbol{\mu} \cdot \mathbf{E}_{\text{inc}}$. This leads to replace $\tilde{\mathbf{E}}^{(1)}$ by $(\boldsymbol{\mu} \cdot \tilde{\mathbf{E}}^{(1)}/\boldsymbol{\mu} \cdot \boldsymbol{\mu})\boldsymbol{\mu}$ in Eq. (5).

Hereafter for simplicity, we focus on the amplitude coefficients of the incident Bloch mode only. The scattering matrix for one atom, which relates the scattered mode amplitudes, a' and b, to the incident ones, a and b' (see Fig. 1), has the following form:

$$\begin{pmatrix} a' \\ b \end{pmatrix} = \begin{bmatrix} t & r' \\ r & t' \end{bmatrix} \begin{pmatrix} a \\ b' \end{pmatrix} = \begin{bmatrix} 1 + \eta\tilde{\mathbf{E}}^{(1)} \cdot \tilde{\mathbf{E}}^{(-1)} & \eta\tilde{\mathbf{E}}^{(1)} \cdot \tilde{\mathbf{E}}^{(1)} \\ \eta\tilde{\mathbf{E}}^{(-1)} \cdot \tilde{\mathbf{E}}^{(-1)} & 1 + \eta\tilde{\mathbf{E}}^{(1)} \cdot \tilde{\mathbf{E}}^{(-1)} \end{bmatrix},$$

(6)

with $\eta = \sigma_0 \frac{-j\epsilon_0 c}{4P} \frac{(2\delta_L/\gamma_0 - j\gamma/\gamma_0)}{4(\delta_L/\gamma_0)^2 + 2(\Omega/\gamma_0)^2 + (\gamma/\gamma_0)^2}$. The Bloch-mode fields are taken at the atom position $\mathbf{r}_A$. Equation (6) has several implications:

– t and t' are equal (reciprocity).
– In sharp contrast to translation-invariant waveguides for which $\tilde{\mathbf{E}}^{(1)} \cdot \tilde{\mathbf{E}}^{(1)} = \tilde{\mathbf{E}}^{(-1)} \cdot \tilde{\mathbf{E}}^{(-1)}$ because of translation symmetry, r and r' are different in general. Thus, the scattering matrices of periodic and translation-invariant waveguides are fundamentally different, and the formulas directly inspired from classical waveguide results in recent works [6,22] clearly overlook the phase difference between r and r'.
– For nonabsorbent dielectric waveguides, since $\tilde{\mathbf{E}}^{(-1)} = -(\tilde{\mathbf{E}}^{(1)})^*$, $r'/\eta = r/\eta$, and $|r'|^2$ and $|r|^2$ are equal. Perhaps counter-intuitively, this holds regardless the atom location in the unit cell of the waveguide.
– For metallic waveguides such as nanoparticle chains that offer deep subwavelength transverse confinements [23], $|r'|^2$ and $|r|^2$ are different.
– For small driving fields, saturation is negligible, and the spectral width is given by γ. As one tunes the band edge near the atomic transition line, the total decay rate is mainly driven by the coupling to the waveguide and becomes proportional to the group index [6].

We consider a periodic nanowire [24] formed by a 1D chain of Si_3N_4 boxes in vacuum. With this example shown in the inset in Fig. 2, our intention is not to provide a thorough discussion of a realistic geometry with a complete design
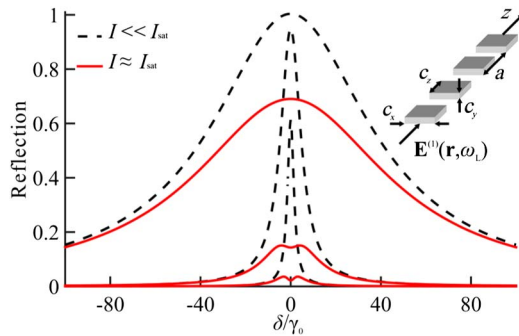

Fig. 2. Reflection spectra for an atom trapped in a sub-λ periodic nanowire (inset) for three values of the group index, $n_g = 3$, 10, and 80. Black dashed curves hold for low laser intensities, and red solid curves for a laser intensity close to the saturation intensity of Cs atoms ($\gamma_0 = 33$ MHz). The calculation is performed for an on-axis atom in the middle of the air gap, and for $c_x = 500$ nm, $c_y = 100$ nm, $c_z = 220$ nm, and $a = 310$ nm.

including the evaluation of Casimir–Polder forces and trapping forces with detuned lasers [6,22]. Rather, we intend to illustrate the meaning behind Eq. (6) on a simple example. All dimensions are given in the caption. For TE-like horizontal polarization, the nanowire supports a truly guided Bloch mode, and the conduction-band-edge energy coincides with the Cesium D_2 transition line at 852 nm.

Figure 2 shows typical reflection spectra obtained for three values of the group index $n_g = 3$, 10, and 80. At resonance and low excitation powers (black dashed curves), the photon is completely reflected for large n_g's. As the band edge frequency is tuned near the atomic transition frequency, the atom serves as an ultranarrow filter, and the incident laser field is almost completely reflected. The lineshape is the same as when a waveguide is coupled to a monomode cavity [25], but more complex Fano lineshapes can be obtained for multimode waveguides, as can be deduced from Eqs. (5a) and (5b). The red solid curves are obtained for an averaged guided power of ≈ 5 pW. For this power that corresponds to 2.1 mW/cm^2, saturation effects cannot be neglected [26], and the coherent backscattering at the atomic transition frequency is reduced. At larger incident powers ($\Omega \gg \gamma_0$), most photons are directly transmitted, $|t|^2 \to 1$. Interestingly, we observe that saturation effects for the same averaged guided power are prominent at small n_g's. This holds because the external Rabi frequency scales as $\Omega \propto n_g^{1/2}$, whereas the spontaneous emission rate of the atom scales at a much faster rate, $\gamma \propto n_g$.

The main difficulty of the previous treatment comes from calculating the emission decay into radiation modes [12], which requires accurate outgoing wave conditions in the periodic directions. Although PML-like absorbing boundaries in periodic media have been recently optimized [27], any termination breaks periodicity, and numerical calculations relying on a 3D sampling is inevitably contaminated by termination backscattering, especially for small group velocities. Thus in practice, it is easier to consider finite waveguides. For instance, in a recent theoretical work [22], the classical Green's tensor is not calculated for fully-periodic (infinite) waveguides, but for finite ones formed by a finite number of unit cells. Consequently, the predicted spontaneous decay rate displays a series of spurious resonance peaks, which depends on the somewhat arbitrary choice of the waveguide length and terminations and from which it is difficult to infer the actual decay rate of the periodic system.

We overcame the issue by using an approach that does not rely on numerical meshing in the periodic direction, but rather on an *analytical* expansion in the QNBM basis [12]. The approach proposes virtually "exact" predictions for γ, but in turn it relies on uncommon advanced numerical tools and on calculations that need to be repeated for every atom position. Thus, it is advantageous to consider an approximate treatment, in which the spontaneous decay rate γ_{rad} in radiation Bloch modes is assumed to be equal to the emission rate in vacuum

$$\frac{\gamma}{\gamma_0} \approx 1 + \frac{3\pi c}{2\omega^2 P}|\tilde{\mathbf{E}}^{(1)}(\mathbf{r}_A)|^2.$$

(7)

Together, Eqs. (5a), (5b) and (6) analytically predict the spectral response for any driving frequency and atom location. The prediction only requires the knowledge of the driving electrical-field distribution, which is easily calculated for dielectric or metallic structures with Bloch-mode solvers.
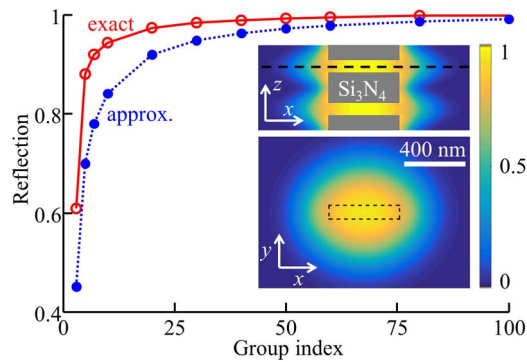
Fig. 3.   Approximate treatment. Reflection spectra at low excitation powers for an atom in the middle of the air gap and matched in frequency with the driving field. The red solid and blue dotted curves are obtained with "exact" and approximate treatments. The insets show the reflectance as a function of the atom position in the x–z and x–y (indicated by a dashed line in the top inset) symmetry planes, predicted with Eq. (7) for $n_g = 40$. In the top inset, gray regions represent the Si_3N_4 boxes. On the bottom, the dashed rectangle indicates the position of the Si_3N_4 box.

Figure 3 provides an evaluation of the error introduced by Eq. (7) as a function of the group index n_g of the driving field for an atom trapped in the middle of the air gap between two Si_3N_4 boxes and matched in frequency. As expected, the error weakens at large n_g's. It comes from the fact that the decay into all radiation modes is smaller than the decay in vacuum ($\gamma_{rad} < \gamma_0$) [8]; we have checked that the "exact" data displayed with red circles can be perfectly reproduced by replacing 1 by 0.4 in Eq. (7). This evidences that accurate predictions can be obtained with Eq. (7) and with an additional "exact" calculation performed at a single frequency. Equation (7) offers a high degree of simplicity. For illustration, we calculate the reflection at zero detuning as a function of the atom position for $n_g = 40$. The results (see inset) are likely to be inaccurate for small reflectance, but their merit is to rapidly visualize atom positions that offer large couplings.

Because they are directly expressed into the natural electromagnetic eigenstates of the waveguide, Bloch-mode scattering matrices of single atoms are an important ingredient toward the analysis of collective effects [7] resulting from the strong interaction between slow photons and a collection of dilute atoms. Used at low excitation powers in conjunction with 2×2 Bloch-mode scattering-matrix-product algorithms [10], Eq. (6) allows the study of realistic waveguides, with lengths of a few hundred period [10], terminated with arbitrary facet reflectivities [9], or lossy due to absorption or to fabrication imperfections [10]. The additional flexibility brought by the analytical formula, Eq. (7), allows fast computations that may help interpretations when some physical parameters are tuned, such as the atom positions that are not precisely known in experiments. As a final remark, note that Eq. (6) is valid for atom–field interactions that are mediated not only by propagative photons in the band, but also for photons with energies within the gap, since the normalization does not rely on energy considerations.

REFERENCES

1. P. Lodahl, S. Mahmoodian, and S. Stobbe, Rev. Mod. Phys. **87**, 347 (2015).
2. F. Le Kien, V. I. Balykin, and K. Hakuta, Phys. Rev. A **70**, 063403 (2004).
3. F. Le Kien, S. Dutta Gupta, V. I. Balykin, and K. Hakuta, Phys. Rev. A **72**, 032509 (2005).
4. F. Warken, E. Vetsch, D. Meschede, M. Sokolowski, and A. Rauschenbeutel, Opt. Express **15**, 11952 (2007).
5. J. D. Thompson, T. G. Tiecke, N. P. de Leon, J. Feist, A. V. Akimov, M. Gullans, A. S. Zibrov, V. Vuletić, and M. D. Lukin, Science **340**, 1202 (2013).
6. A. Goban, C.-L. Hung, S.-P. Yu, J. D. Hood, J. A. Muniz, J. H. Lee, M. J. Martin, A. C. McClung, K. S. Choi, D. E. Chang, O. Painter, and H. J. Kimble, Nat. Commun. **5**, 3808 (2014).
7. A. Goban, C.-L. Hung, J. D. Hood, S.-P. Yu, J. A. Muniz, O. Painter, and H. J. Kimble, arXiv:1503.04503 (2015).
8. G. Lecamp, P. Lalanne, and J. Hugonin, Phys. Rev. Lett. **99**, 023902 (2007).
9. C. Sauvan, P. Lalanne, and J. P. Hugonin, Phys. Rev. B **71**, 165118 (2005).
10. A. Baron, S. Mazoyer, W. Smigaj, and P. Lalanne, Phys. Rev. Lett. **107**, 153901 (2011).
11. J. T. Shen and S. Fan, Opt. Lett. **30**, 2001 (2005).
12. G. Lecamp, J. P. Hugonin, and P. Lalanne, Opt. Express **15**, 11042 (2007).
13. G. Grynberg, A. Aspect, and C. Fabre, *Introduction to Quantum Optics: From the Semi-classical Approach to Quantized Light* (Cambridge University, 2010).
14. K. Kojima, H. F. Hofmann, S. Takeuchi, and K. Sasaki, Phys. Rev. A **68**, 013803 (2003).
15. V. S. C. Managa Rao and S. Hughes, Opt. Lett. **32**, 304 (2007).
16. D. E. Chang, A. S. Sørensen, E. A. Demler, and M. D. Lukin, Nat. Phys. **3**, 807 (2007).
17. A. Gonzalez-Tudela, D. Martin-Cano, E. Moreno, L. Martin-Moreno, C. Tejedor, and F. J. Garcia-Vidal, Phys. Rev. Lett. **106**, 020501 (2011).
18. L. Zhou, Z. R. Gong, Y. Liu, C. P. Sun, and F. Nori, Phys. Rev. Lett. **101**, 100501 (2008).
19. Y. Chang, Z. R. Gong, and C. P. Sun, Phys. Rev. A **83**, 013825 (2011).
20. X.-W. Chen, V. Sandoghdar, and M. Agio, Phys. Rev. Lett. **110**, 153605 (2013).
21. A. W. Snyder and J. D. Love, *Optical Waveguide Theory* (Springer, 1984).
22. C.-L. Hung, S. M. Meenehan, D. E. Chang, O. Painter, and H. J. Kimble, New J. Phys. **15**, 083026 (2013).
23. S. A. Maier, P. G. Kik, H. A. Atwater, S. Meltzer, E. Harel, B. E. Koel, and A. A. G. Requicha, Nat. Mater. **2**, 229 (2003).
24. R. Halir, P. J. Bock, P. Cheben, A. Ortega-Moñux, C. Alonso-Ramos, J. H. Schmid, J. Lapointe, D.-X. Xu, J. G. Wangüemert-Pérez, Í. Molina-Fernández, and S. Janz, Laser Photon. Rev. **9**, 25 (2015).
25. E. Waks and J. Vuckovic, Opt. Express **13**, 5064 (2005).
26. D. A. Steck, "Cesium D Line Data," Los Alamos National Laboratory, 2010, http://steck.us/alkalidata.
27. D. Pissoort and F. Olyslager, IEEE Antennas Wirel. Propag. Lett. **2**, 281 (2003).